Al-Khwarizmi Engineering Journal, Vol. 4, No. 3, PP 98-107 (2008)

Al-Khwarizmi Engineering Journal

Heating and Melting Model Induced by Laser Beam in Solid Material

Faiz F. Mustafa

Department of Manufacturing Operations Engineering /Al-Khwarizmi College of Engineering
University of Baghdad

(Received 2 March 2008; accepted 15 June 2008)

Abstract

An analytical method and a two-dimensional finite element model for treating the problem of laser heating and melting has been applied to aluminum 2519T87and stainless steel 304. The time needed to melt and vaporize and the effects of laser power density on the melt depth for two metals are also obtained. In addition, the depth profile and time evolution of the temperature before melting and after melting are given, in which a discontinuity in the temperature gradient is obviously observed due to the latent heat of fusion and the increment in thermal conductivity in solid phase. The analytical results that induced by $10.6\mu m$ laser irradiation is in good agreement with numerical results.

Keywords: Laser; Heating; Melting; Finite element method; Non-linear heat transfer

1. Introduction

High power density, such as laser beam, has been increasingly utilized in industrial manufacturing. The process of laser beam in solid material offers a great potential for the new product design, for example, welding, cutting of metals, drilling of holes, laser shock hardening and laser glazing. When a high power laser irradiates a material surface, a part of the laser energy is absorbed and conducted into the interior of the material. If the absorbed energy is high enough, the material surface will melt and even vaporize. The study of laser induced heating and melting has attracted great interest [1–7] and the results obtained are of great importance for achieving high quality materials processing with lasers.

To simplify the mathematical problem, it is necessary to assume that the process of laser heating and melting is a linear process, that is to say, the physical parameters of the material, including density, thermal conductivity, thermal capacity, optical absorptivity, etc., are independent of the temperature. In this study, a one-dimensional heat conduction problem is solved approximately in the solid and liquid regions by assuming that the thermo-physical properties of the material are independent of the temperature.

Numerical simulation of laser heating and melting with two dimensional finite element methods has been used to evaluate temperature distribution and other variables. A nonlinear transient thermal analysis was performed using temperature dependent material properties used to evaluate temperature distribution

The computations of the depth profile and time evolution of the temperature before melting as well as after melting are carried out for the two materials, the variation of the melt depth with time, the effects of the laser power density on the melt depth and the irradiation time on melting and vaporization are calculated.

2. Mathematical Model

The geometry of laser irradiation and the resulting liquid and solid regions are shown in Fig. 1. The diameter of the laser beam is broad enough compared to the molten region and the thickness of the material is much greater than the

thermal penetration depth, so that the problem can be solved in one dimension and a semi-infinite model may be accepted. The analytical solution applied to aluminum and stainless steel, the thermo-physical parameters in solid and liquid phases are shown in Table 1 were taken from [8-9]. Accordingly the surface of the material reaches the fusion point or not, the whole process of laser induced heating and melting in the material is divided into two steps: before melting and after melting.

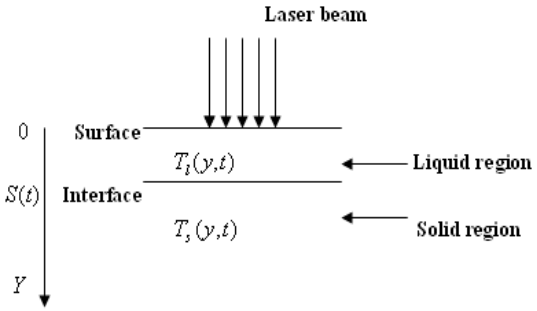


Fig. 1. The Geometry of Laser Irradiation.

Table 1
Thermophysical Parameters and Absorptivity for Materials [8-9].

Material properties	Aluminum (2519T87)	Stainless-steel (304)
$\rho_s(kg/m^3)$	2823	7860
$\rho_L(kg/m^3)$	2485	6980
$C_s(J/kgK)$	896	465
$C_L(J/kgK)$	1080	691
$K_s(W/mK)$	100	53
$K_L(W/mK)$	238	120
$T_m(K)$	933	1811
$T_V(K)$	2793	3134
$L(10^5 kg^{-1})$	3.88	3.65
A_s	0.0588	0.386
A_L	0.064	0.346

2.1. Step A. Before Melting

The thermal conduction model can be described by the following equations before the temperature of the surface reaches the fusion point:

$$\frac{\partial^2 T_S(y,t)}{\partial^2 y} - \frac{1}{\lambda_S}\frac{\partial T_S(y,t)}{\partial t} = 0, \quad 0 \le y \le \infty, \quad \ldots(1)$$

$$-K_S \frac{\partial T_S(y,t)}{\partial y} = A_S I, \qquad y = 0, \qquad \ldots(2)$$

$$T_S(y,t) = T_\circ, \qquad y \to \infty, \qquad \ldots(3)$$

$$T_S(y,t) = T_\circ, \qquad t = 0, \qquad \ldots(4)$$

where T_S, K_S, λ_S and A_S are the temperature, thermal conductivity, thermal diffusivity and absorptivity of the solid phase respectively. $T_\circ$ is the ambient temperature and I is the power density of laser beam.

We first assume a temperature profile, which satisfies the boundary condition (3):

$$T_S(y,t) = T_W(t)e^{-y/\delta(t)}, \qquad \ldots(5)$$

where $T_W(t)$ represents the temperature of the surface and $\delta(t)$ is a temporal function representing the temperature penetration depth in the solid. Substituting expression (5) into Eqs. (2) and (1), we get the following relations:

$$\frac{dT_W(t)}{dt} = \frac{\lambda_S}{\delta^2(t)}T_W(t), \qquad \ldots(6)$$

$$T_W(t) = \frac{A_S I}{K_S}\delta(t), \qquad \ldots(7)$$

According to Eqs. (6) and (7), one gets

$$T_W(t) = T_\circ + \frac{A_S I}{\sqrt{C_S \rho_S K_S}}(2t)^{1/2}, \qquad \ldots(8)$$

$$\delta(t) = \sqrt{2\lambda_S t}. \qquad \ldots(9)$$

2.2 Step B. After Melting

The thermal conduction equations in liquid and solid regions can be described as

$$\frac{\partial^2 T_L(y,t)}{\partial^2 y} - \frac{1}{\lambda_L}\frac{\partial T_L(y,t)}{\partial t} = 0, \; 0 \le y \le S(t), \quad \ldots(10)$$

$$\frac{\partial^2 T_S(y,t)}{\partial^2 y} - \frac{1}{\lambda_S}\frac{\partial T_S(y,t)}{\partial t} = 0, \; S(t) \le y \le \infty \quad \ldots(11)$$

with boundary conditions

$$-K_L \frac{\partial T_L(y,t)}{\partial y} = A_L I, \quad y = 0, \qquad \ldots(12)$$

$$T_S(y,t) = T_L(y,t) = T_{m,} \qquad y = S(t), \quad \ldots(13)$$

$$\rho_S L \frac{dS(t)}{dt} = K_S \frac{\partial T_S(y,t)}{\partial y} - K_L \frac{\partial T_L(y,t)}{\partial y}, \quad \ldots(14)$$

$$T_S(y,t) = T_\circ, \qquad y \to \infty \quad \ldots(15)$$

and initial condition

$$S(t) = 0, \qquad t = t_m, \quad \ldots(16)$$

where T_i, K_i and $\lambda_i = K_i / C_i \rho_i$ are temperature, thermal conductivity and thermal diffusivity of the i th phase respectively ($i = s$ (solid phase) or l (liquid phase)), ρ_i and C_i are the density and heat capacity of the i th phase. A_L is the absorptivity of liquid phase, T_m is the melting point and L is the fusion latent heat of the irradiated material, $S(t)$ is the position of the interface between solid phase and liquid phase.

The temperature profiles in liquid region and solid region are assumed as

$$T_L(y,t) = T_m(t) e^{-y/\delta_l(t)} \quad \ldots(17)$$

$$T_S(y,t) = T_m e^{-y-S(t)/\delta_S(t)} \quad \ldots(18)$$

which satisfy Eqs. (13) and (15), $\delta_L(t)$ and $\delta_S(t)$ are two temporal functions representing the temperature penetration depth in liquid and solid regions. Satisfying Eq. (10) at $y = 0$ by using expression (17) and Eq. (11) at $y = S(t)$ by using expression (13), we obtain

$$\frac{dT_W(t)}{dt} - \frac{\lambda_L T_W(t)}{\delta_L^2(t)} = 0, \quad \ldots(19)$$

$$\frac{dS(t)}{dt} = \frac{\lambda_S}{\delta_S(t)}. \quad \ldots(20)$$

Substituting expression (17) into Eq. (12), we get

$$\frac{K_L T_W(t)}{\delta_L(t)} = A_L I. \quad \ldots(21)$$

Substituting expressions (17) and (18) into Eq. (14) and by using Eq. (13), we obtain

$$\frac{dS(t)}{d(t)} = \frac{T_m}{\rho_S L}\left(\frac{K_L}{\delta_L(t)} - \frac{K_S}{\delta_S(t)}\right). \quad \ldots(22)$$

According to Eqs. (19)–(22), the following relations are obtained:

$$T_W(t) = \left[\frac{2\lambda_L A_L^2 I^2}{K_L^2} t + C_\circ\right]^{1/2}, \quad \ldots(23)$$

$$\delta_L(t) = \frac{K_L}{A_L I}\left[\frac{2\lambda_L A_L^2 I^2}{K_L^2} t + C_\circ\right]^{1/2}, \quad \ldots(24)$$

$$\delta_S(t) = \frac{\rho_S L}{A_L I T_m}\left(\lambda_S + \frac{T_m K_S}{\rho L}\right)\left[\frac{2\lambda_L A_L^2 I^2}{K_L^2} t + C_\circ\right]^{1/2}, \quad \ldots(25)$$

$$S(t) = \frac{K_L}{A_L I}\left[\frac{2\lambda_L A_L^2 I^2}{K_L^2} t + C_\circ\right]^{1/2} \ln\frac{\left[2\lambda_L A_L^2 I^2 t / K_L^2 + C_\circ\right]^{1/2}}{T_m}, \quad \ldots(26)$$

where $C_\circ = T_m^2 - \dfrac{\lambda_L K_S^2 A_L^2}{\lambda_S K_L^2 A_S^2}(T_m - T_\circ)^2$.

3. Finite Element Modeling

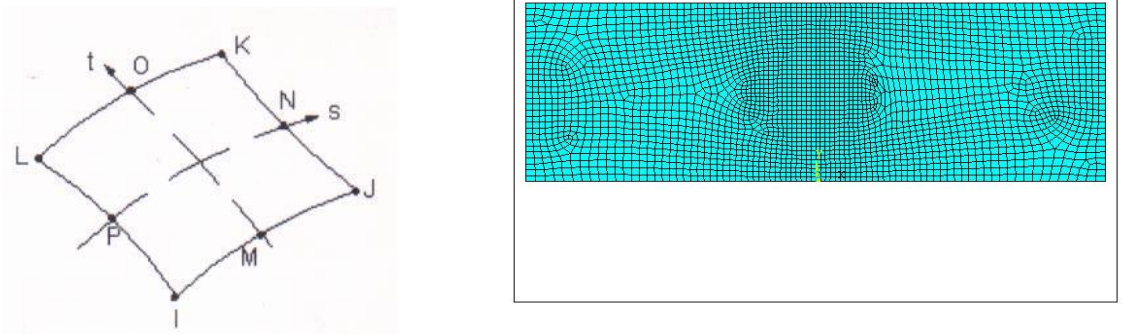
During the laser irradiation many mechanisms are taking place in the basin material; a very narrow zone under the laser beam is suddenly heated, vaporized and locally fused. A two-dimensional finite element model was used to simulate the laser processes on the depth of the solid material using the commercial code ANSYS (9). The geometry of the structure, shown in Fig 2-a, was modeled using a two dimensional solid 8-nod element to simulate the laser processes on the depth of the solid material. The width of the material is broad enough compared to the molten region and the depth of the material is much greater to than the thermal penetration depth.

The accuracy of the FE method depends upon the density of the mesh used in the analysis. The laser spot temperature is higher than the melting point of the material, and it drops sharply in regions away from the laser spot. Therefore in order to obtain the correct temperature field in the region of high temperature gradients it was necessary to have a more refined mesh close to the laser spot, while in regions located away a more coarse mesh was used as shown in Fig. 2-b. The final mesh was the result of compromise between computing time and accuracy. A transient heat transfer analysis was performed with an appropriate time-stepping scheme to achieve fast convergence of the solution and reasonable accuracy.

The thermal analysis was conducted using temperature dependent thermal material properties the values of these properties for aluminum 2519 T87and stainless steel 304 are shown in Table 2 were taken from [10-11]. The governing partial differential equation for the transient heat conduction is

$$\left[K(T)\left(\frac{\partial^2 T}{\partial x^2}\right) + \left(\frac{\partial^2 T}{\partial y^2}\right)\right] + Q^{\bullet} = \rho(T) C_P(T)\left(\frac{\partial T}{\partial t}\right) \quad \ldots(27)$$

where x, y are the Cartesian coordinates, $Q^{\bullet}$ the internal heat generation, ρ the density, K the thermal conductivity and C_P the specific heat are function of temperature T. The temperature dependent material properties were inserted in FE code in the table form.



(a) **(b)**

Fig. 2. (a) 2-D Solid 8-nod Element. (b) 2-D Finite Element Geometry and Mesh.

3.1 Heat Input

The heat input is generally calculated from the energy supplied, during laser irradiates at the solid material. The geometry considered in this dissertation is a finite, rectangular work-piece irradiated by a laser beam impinging on its surface and subjected to convection and radiation heat losses. A laser power *P* is assumed to have a uniformly distributed over a circular area of radius ω on the surface of a work-piece, so that a laser beam is assumed to have a uniform intensity distribution *I* defined as

$$I = P/\pi\omega^2 \qquad \ldots(28)$$

3.2 Boundary and Initial Conditions

During the laser irradiates, the heat was supplied to the specimen surface by the beam laser. This heat is transferred to the metal by the conduction and convection. A part of this heat energy is lost by free convection and radiation. The heat loss by free convection follows Newton's law, where the coefficient of convective heat transfer was assumed to vary with both temperature and orientation of boundary.

$$q_c = \frac{KNu}{L}(T - T_\circ) \qquad \ldots(29)$$

where K is the thermal conductivity of the material, L the characteristic length of the plate (or surface), $T_\circ$ the ambient temperature, and Nu Nusselt number defined by

$$Nu = 5.67\,\mathrm{Pr}^{1/3}\,Gr^{1/3} \qquad \ldots(30)$$

where Pr is the Prandtl number and Gr is the Grashof number, both of them being functions of ambient air properties and temperature differences between the surface and the environment.

Heat loss due to thermal radiation between the spacemen and environment are important when the temperature difference is high. This radiation was modeled by the standard Stefan-Boltzman relation

$$q_r = \varepsilon\sigma(T^4 - T_\circ^4) \qquad \ldots(31)$$

where ε is the heat emissivity and σ the Stefan-Boltzman constant. Radiation is assumed from the surface to the surroundings. The material is assumed to be at room temperature.

4. Results and Discussions

We apply the above analytical solutions to aluminum and stainless steel. Table 2 shows their thermophysical parameters in solid and liquid phases and their absorptivity at wave length $10.6\mu m$ laser irradiation.

Table 2
Variation of Thermal Properties with Temperature [10-11].

Temp (°C)	k (W/m/c) Thermal conductivity		Cp (J/Kg/c) Specific heat		ρ (Kg/m^3) Density	
	S.S	AL	S.S	AL	S.S	AL
0	53	100	465	896	7860	2823
100	52	140	485	915	7721	2754
200	50	160	494	950	7648	2705
300	46	155	509	952	7603	2654
400	42	145	529	1080	7670	2613
500	39	145	562	=	7635	2559
600	36	180	582	=	7405	2500
700	32	238	638	=	7365	2485
800	25	238	691	=	7330	2485
900	27	-	690	-	7303	-
1000	28	-	688	-	7272	-
1100	29	-	=	-	7235	-
1200	30	-	=	-	7210	-
1300	31	-	=	-	7170	-
1400	32	-	=	-	7131	-
1500	70	-	=	-	7103	-
1600	120	-	=	-	7042	-
1700	120	-	=	-	6980	-

4.1. Melt Depth

The propagation of the solid–liquid interface expressed by Eq. (26) shows that the melt depth increases rapidly at the beginning of laser irradiation and then slowly after a certain time. Such a trend is also observed in experimental studies for the laser drilling of aluminum [12]. The Mathematical and finite element calculated melt depth evolution of aluminum induced by $10.6\mu m$ laser irradiation compared to the experimental data [12] is shown in Fig. 3. This figure shows a good agreement between the theory and the experiment for irradiation times less than about 4sec, but some deviations appear as the time increases. In fact, vapor and plasma will occur at large irradiation times; which block the incident laser light and absorb a portion of laser energy, but such effects are ignored in this work. As a result, the theoretical results seem to overestimate the melt depth for large irradiation times. Therefore, the model expressed by Eq. (26) is accurate when the vapor or plasma is not very strong, which is usually the case at the beginning of the irradiation process.

The Mathematical and finite element variations of melt depth with $10.6\mu m$ laser irradiation time for aluminum and stainless steel are shown in Fig. 4. At the beginning, the melting velocity is high and then decreases to a low value. The trend is the same as that observed in experimental studies. Some deviations appear between mathematical and finite element especially at the time increases because the temperature independences thermal material properties of the mathematical model.

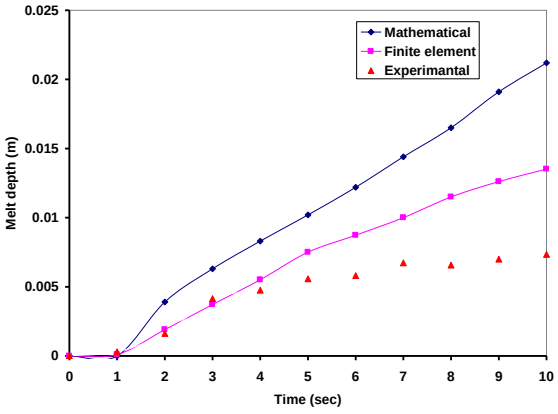


Fig. 3. Melt Depth Evaluation of Aluminum.

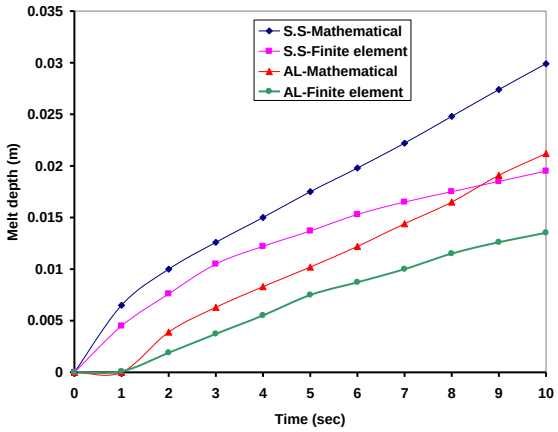


Fig. 4. Melt Depth Evaluation of Stainless-Steel and Aluminum I= 10^8 W/m^2.

4.2. Temperature Profile and Evolution

The mathematical and finite element temperature fields as the functions of depth for aluminum at different irradiation times are plotted in Fig. 5. (a) and (b). The curves 1 and 2 represent the temperature distribution in the solid before melting, while the curves 3 and 4 represent that after melting. For both models the temperature within the liquid phase decreases rapidly from the surface temperature to the melting temperature. Beyond the solid–liquid interface in the solid phase region, the temperature decreases to the ambient temperature with a relatively gradual gradient. Such a discontinuity in the temperature gradient is obviously observed due to the latent heat of fusion and the increment in thermal conductivity in the solid phase. It is also seen from the figure that the evolution of the surface temperature after melting is much faster than before melting, which results from the higher absorptivity and lower thermal conductivity in liquid phase. Fig. 6. (a) and (b), gives the finite element temperature profile for aluminum and stainless steel at the same power density I= 10^8 W/m^2 for different time irradiate, we can see with the different time the melt depth of aluminum are less than that of stainless steel due to high thermal conductivity and low absorptivity.

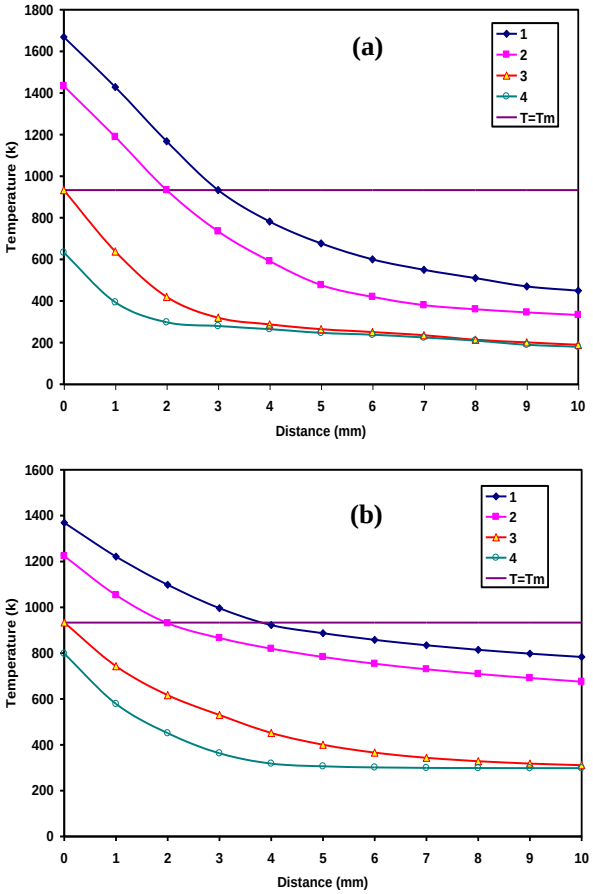
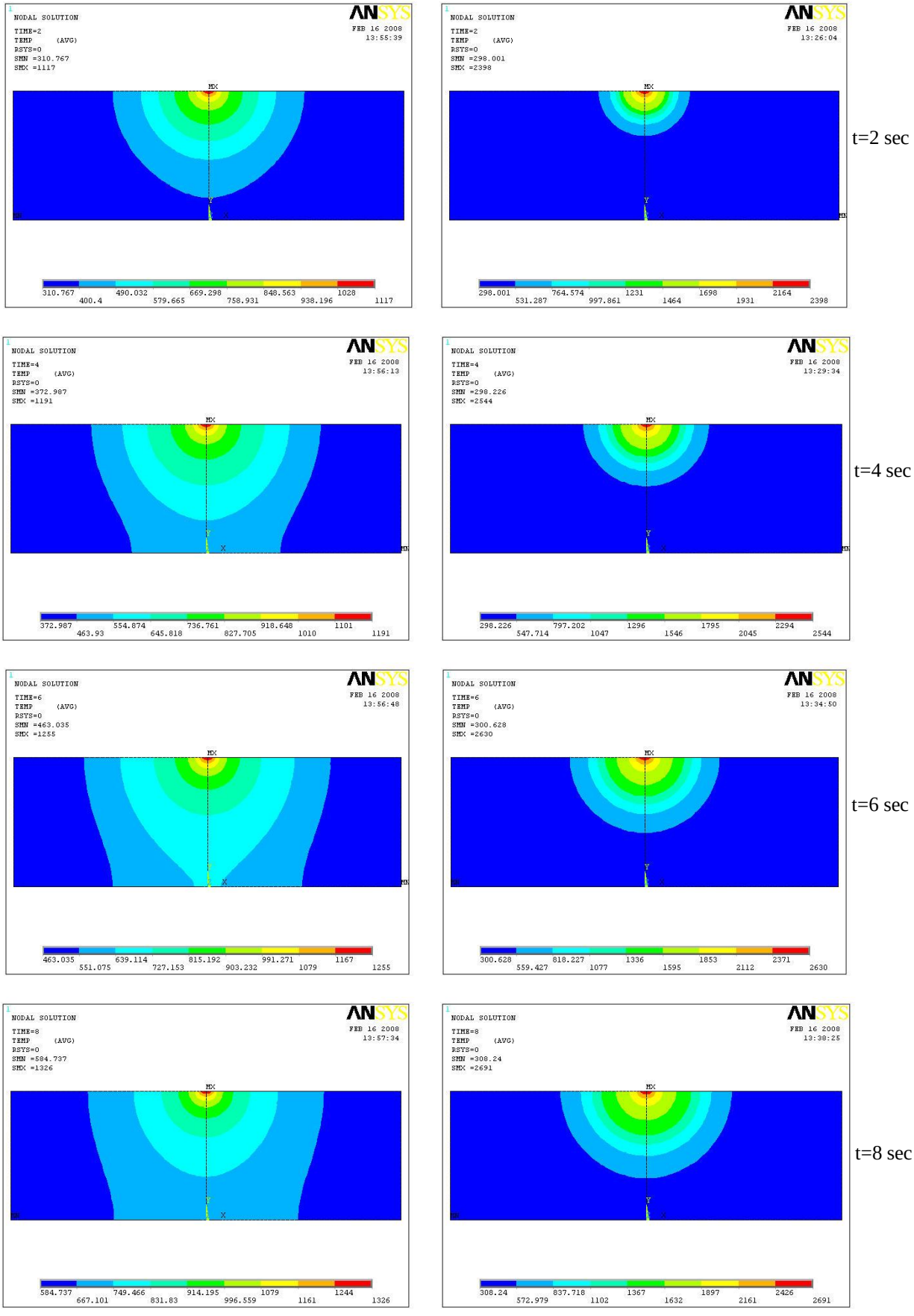


Fig. 5. Temperature Distribution of Aluminum at Different Irradiation Time I= 7*10^8 W/m^2.
(a) Mathematical, (b) Finite Element.

4.3. The Effects of Power Density on Melt Depth

The variations of melt depth versus incident power density for a given laser irradiation time for aluminum and stainless steel are plotted in Fig. 7. In the two cases (mathematical and finite element), the melt depth increases rapidly with increasing power density when the power density is low, and increases slowly at higher power densities. It is shown that the melt depths of aluminum are less than that of stainless steel at low power density, while greater than that at higher power densities. Aluminum has high thermal conductivity and low absorptivity, so that they are difficult to melt compared to stainless steel at low laser power density. With the increment of incident power density, more laser energy can be conducted to the solid–liquid interfaces of aluminum due to their higher thermal conductivity so that more laser energy needs to be used to achieve melting. Therefore, the melt depths of aluminum will exceed these of stainless steel at higher power density.



(a) **(b)**

Fig. 6. Temperature Distribution During Laser Irradiation at Different Times, $I=10^8$ W/m^2. (a) Aluminum, (b) Stainless Steel.

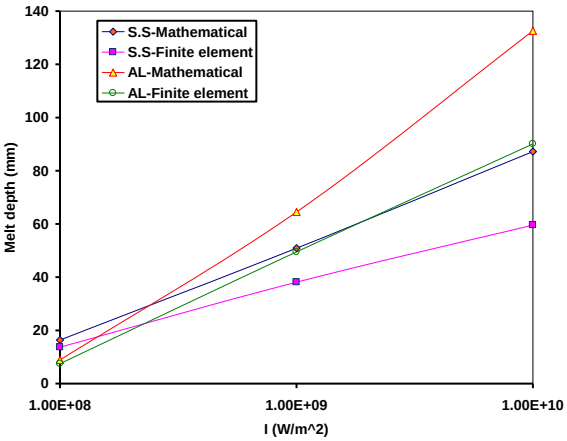


Fig. 7. Influence of Power Density on Melt Depth at Time= 5 sec.

4.4. The Time for Surface to Melt and Vaporization

Let $T_W(t)$ in Eq. (8) equal the fusion temperature T_m. The time for the surface reaching the melting point t_m is

$$t_m = \frac{(T_m - T_\circ)^2 C_S \rho_S K_S}{2(A_S I)^2} \qquad \ldots(32)$$

Let $T_W(t)$ in Eq. (23) equal the vaporization temperature T_V. The time for the surface reaching the vaporization point t_v is

$$t_v = \frac{(T_V^2 - C_\circ)K_L^2}{2(A_L I)^2 \lambda_L} \qquad \ldots(33)$$

The results of two metals are shown in Table 3. It is shown that stainless-steel needs least time to reach fusion temperature and vaporization temperature then aluminum due to its low thermal conductivity although it has relatively high fusion and vaporization temperatures.

Table 3
The Time Needed to Melt and Vaporize for Materials at Different Power Densities.

$I(W/m^2)$		10^8	10^9	10^{10}
Melting time(s)	Al	1.175	1.175*10^-2	1.170*10^-4
	S.S	0.148	0.148*10^-2	0.148*10^-4
Vaporizing time(s)	Al	55.51	55.51*10^-2	56.01*10^-4
	S.S	1.730	1.730*10^-2	1.730*10^-4

5. Conclusions

An analytical method for treating the problem of the laser heating and melting is considered in this paper by suggesting a simple and reasonable temperature profile and compared with a two dimensional finite element model. We apply the two methods to aluminum 2519T87 and stainless steel 403. The temperature profile and evolution of aluminum before melting as well as after melting is described. A discontinuity in the temperature gradient is obviously observed due to the latent heat of fusion and the increment in thermal conductivity in solid phase. The calculated melt depth evolution of aluminum is in good agreement with the experimental results. The effects of laser power density on the melt depths for two metals are also obtained. It can also be concluded that stainless steel needs least time to reach fusion temperature and vaporization temperature than aluminum due to its low thermal conductivity although it has relatively high fusion and vaporization temperatures.

References

[1] El-Adawi MK, El-Shehawey EF. Heating a slab induced by a time-dependent laser irradiation—An exact solution. J. Appl Phys 1986; 60 (7): 2250–5.
[2] Hassan AF, El-Nicklawy MM, El-Adawi MK. A general problem of pulse laser heating of a slab. Opt Laser Technol 1993; 25 (3): 155–62.
[3] Rantala TT, Levoska J. A numerical simulation method for the laser-induced

temperature distribution. J. Appl. Phys. 1989; 65 (12): 4475–9.

[4] Armon E, Zvirin Y, Laufer G. Metal drilling with a CO2 laser beam. I. Theory. J Appl. Phys 1989; 65(12): 4995–5002.

[5] Kar A, Mazumder J. Two-dimensional model for material damage due to melting and vaporization during laser irradiation. J. Appl. Phys. 1990; 68: 3884–91.

[6] V. A. Karkhin, V. A. Lopota, and N. O. Palova. Effect of phase transformations on residual stresses in laser welding. Welding International 2003 17 (8) 645–649

[7] Han GuoMing, Zhao Jian, Li JianQang. Dynamic simulation of the temperature field of stainless steel laser welding. School of Material Science and Engineering, Tianjin University, China, 8 June 2005.

[8] S.A. Tsirkas, P. Papanikos, Th. Kermanidis. Numerical simulation of the laser welding process in butt-joint specimens. J Materials Processing Technology 2003; 134:59-69.

[9] Justin D. Francis. Welding Simulations of Aluminum Alloy Joints by Finite Element Analysis. Master of Science in Aerospace Engineering April 2002 Blacksburg, Virginia

[10] A. Anca, A. Cardona, and J.M. Risso. 3D-Thermo-Mecanical Simulation of Welding Processes. Centro Internacional de M´etodos Computacionales en Ingenier´ıa (CIMEC), Bariloche, Argentina, November 2004.

[11] D. Berglund, L.E. Lindgren and A. Lundbäck. Three-Dimensional Finite Element Simulation of Laser Welded Stainless Steel Plate. Computer Aided Design, Luleå University of Technology, 97187 Luleå, Sweden, 2004.

[12] Armon E, Zvirin Y, Laufer G. Metal drilling with a CO2 laser beam. II. Experiment. J. Appl. Phys. 1989; 65 (12): 5003–8.

النموذج الحراري والانصهاري الناتج من الحزمة الليزرية على المواد الصلبة

فائز فوزي مصطفى
قسم هندسة عمليات التصنيع/ كلية هندسة الخوارزمي/ جامعة بغداد

الخلاصة

لوصف ظاهرة ارتفاع الحرارة والوصول الى درجة الانصهار الناتج من حزمة ليزرية مسلطة على جسم صلب، تم استخدام نموذج رياضي احادي البعد بالاضافه الى استخدام طريقة العناصر المحدده ثنائية البعد لكل من مادة الالمنيوم نوع (2519T87) والحديد المقاوم للصداء نوع (304). تم حساب الوقت اللازم للوصول ال ى درجة الانصهار والتبخر وتأثير كثافة طاقة حزمة الليزر على عمق الانصهار الحاصل لكلا المادتين. هذا بالاضافه الى العمق الجانبي مع تغير درجات الحرارة لمختلف الازمان قبل وبعد حدوث عملية الانصهار، حيث لوحظ عدم استمرارية انسيابية تدرج درجات الحرارة بشكل واضح عند الانتقال من الطور السائل الى الطور الصلب وذلك بسبب الحرارة الكامنة للانصهار والزيادة الحاصلة في معامل التوصيل الحراري للطور الصلب عما هو عليه في الطور السائل. لقد اوضحت النتائج الرياضيه توافق جيد مع النتائج العددية باستخدام طريقة العناصر المحددة الناتجة من للحزمة الليزرية بطول موجي $10.6\mu m$.